Supporting Information

Photo-CIDNP-Enhanced ^{19}F NMR for Rapid Protein Conformation and Ligand Binding Analysis

Zhaofei Chai,[a,b‡*] Weixuan Wang,[a,b‡] Qiong Wu,[a,b‡] Xiaoli Liu,[a,b] Jiawen Chen,[a,b] Yanqi Xu,[a,b] Guohua Xu,[a,b] Xiuchao Zhao,[a,b] Xin Zhou,[a,b] Ling Jiang,[a,b] Maili Liu,[a,b] Conggang Li[a,b*]

[a] State Key Laboratory of Magnetic Resonance Spectroscopy and Imaging, National Center for Magnetic Resonance in Wuhan, Wuhan National Laboratory for Optoelectronics, Wuhan Institute of Physics and Mathematics, Innovation Academy for Precision Measurement Science and Technology, Chinese Academy of Sciences, Wuhan 430071, China

[b] Graduate University of Chinese Academy of Sciences, Beijing 100049, China

[+] Z. Chai, W. Wang and Q. W contributed equally to this work.

* E-mail: czfei@wipm.ac.cn (Z. Chai) and conggangli@wipm.ac.cn (C. Li)

Table of Contents

1 Materials and Methods

1.1 Materials and Instrumentation

All commercially available reagents and solvents were used as received without further purification. NMR spectra were acquired on a Bruker Avance spectrometer operating at 700 MHz equipped with a triple-resonance cryogenic probe. Light was provided by a 488 nm laser (FC-488nm-3W-FH80409, Changchun New Industries Optoelectronics Tech. Co., Ltd., China) coupled through a fiber optic system into a glass coaxial insert (NI5CCI-B, Norell) positioned 4-5 mm above the NMR receiver coil. The light power at the tip of the coaxial insert was calibrated to be 1.28 W using a thermal power sensor (S425C-L, Thorlabs). All NMR data were processed using Bruker TopSpin 3.6.5 software. Unless otherwise noted, the protein structural images were generated using PyMOL.

1.2 Protein Expression and Purification

Genes for SH3, BD2, GB1(T11W), GB1(T11Y), Pin1, and PDI were cloned and expressed in *Escherichia coli* BL21 (DE3). To facilitate purification, an *N*-terminal hexahistidine (His_6)-tag was incorporated into the constructs for BD2, Pin1, and PDI. For the incorporation of 6-F Trp[1], 6-fluoroindole was added to the culture at a final concentration of 70 mg L^{-1} when the optical density at 600 nm (OD_{600}) reached approximately 0.8. After 10 minutes of further incubation (37 °C, 220 rpm), protein expression was induced by adding isopropyl β-D-1-thiogalactopyranoside (IPTG) (0.5 mM). For the incorporation of 3-F Tyr[2], 3-F Tyr was added to the culture at a final concentration of 70 mg L^{-1} when OD_{600} reached approximately 0.4. IPTG (0.5 mM) was added at an OD_{600} of 0.8-1.0 to induce expression. Protein expression was induced under the following conditions: SH3 at 37 °C for 1.5 h; GB1(T11W) and GB1(T11Y) at 37 °C for 6 h; BD2 at 16 °C for 24 h; Pin1 and PDI at 25 °C for 20 h.

After induction, cells were harvested by centrifugation (6000 × g, 10 min, 4 °C) and lysed by high-pressure homogenization at 4 °C. The lysate was clarified by centrifugation (20,000 × g, 30 min, 4 °C), and the supernatant was collected for purification. SH3, GB1(T11W), and GB1(T11Y) were purified by anion-exchange (DEAE Fast Flow column, GE Healthcare) with buffer A (50 mM Tris, pH 8.0) and buffer B (50 mM Tris, 1 M NaCl, pH 8.0). Fractions containing target proteins were further purified with size exclusion chromatography (HiLoad superdex75 16/600 column, GE healthcare) using buffer C (50 mM Tris, 500 mM NaCl, pH 8.0).

BD2, Pin1 and PDI were purified through a HisTrap Ni-NTA affinity column (GE healthcare) with buffer A (50 mM PB, 1 M NaCl, 1% glycerol, pH 8.0) and buffer B (50 mM PB, 1 M NaCl, 500 mM imidazole, 1% glycerol, pH 8.0). BD2 was further purified through a cation exchange (SP, GE healthcare) with buffer C (50 mM PB, 1 mM TCEP, pH 6.0) and buffer D (50 mM PB, 1 M NaCl, 1 mM TCEP, pH 6.0). Pin1 and PDI were further purified by size-exclusion chromatography (HiLoad superdex75 16/600, GE healthcare) using buffer C (50 mM Tris, 500 mM NaCl, pH 8.0). All proteins were desalted into H_2O using a desalting column (Hiprep^{TM} 26/10 Desalting, GE healthcare), immediately frozen in liquid nitrogen, and subsequently lyophilized. The lyophilized proteins were stored at –80 °C until use.

1.3 Sample Preparation

The photo-CIDNP buffer consisted of 200 mM phosphate buffer (PB, pH 7.4) supplemented with 5 mM glucose, 0.2 μM glucose oxidase, and 0.125 μM catalase.[3] The photosensitizer concentrations were optimized as follows: 20 μM flavin mononucleotide (FMN) with a single scan; 10 μM fluorescein (FL) with a single scan; and 20 μM FL with multiple scans (Figures S1, S4 and S10). Unless otherwise specified, Trp, Tyr, and their monofluorinated analogs were prepared as 10 mM aqueous stock solutions (with pH adjusted using NaOH/HCl as needed for solubility) and diluted to approximately 30 μM for the measurements. The phosphorylated peptide FFpSPR and pCDC25c, as well as the small-molecule ligands GSK-046, RVX-208, BAY-299, GSK-620 and GSK-778, were prepared as 20 mM or 50 mM stock solutions in dimethyl sulfoxide (DMSO), respectively. Protein SNE was measured at ~125 μM to rapidly acquire dark spectra with sufficient SNR, although the use of 10 μM FL at this concentration may lead to saturation, thus potentially underestimating the maximum SNE. Prior to data acquisition, all samples were gently mixed and incubated at 25 °C for at least 30 min to remove dissolved oxygen.

1.4 Photo-CIDNP Experiments

A procedure similar to the previous one was adopted.[4] Generally, the illumination time was optimized to 1.5 s for a single scan, and 0.2 s for multiple scans (other experimental conditions are provided in the figure captions). All ^{19}F NMR experiments were performed at 298 K with proton decoupling. During signal-to-noise ratio (SNR) (0-Hz linebroadening) computation, negative phase

signals (emission) were mathematically converted to positive values for calculation purposes, while maintaining their original negative sign in the final recorded output. The signal-to-noise enhancements (SNEs) were calculated as

$$\mathrm{SNE} = \frac{SNR_{L,1\ scan} - SNR_{D,1\ scan}}{SNR_{D,1\ scan}} = \frac{\frac{SNR_L}{\sqrt{NS_L}} - \frac{SNR_D}{\sqrt{NS_D}}}{\frac{SNR_D}{\sqrt{NS_D}}} = \frac{\frac{\sqrt{NS_D}}{\sqrt{NS_L}} SNR_L - SNR_D}{SNR_D}$$

where NS_L and NS_D represented the number of scans for the light spectra and dark spectra, respectively, while SNR_L and SNR_D denoted the corresponding signal-to-noise ratios. To ensure comparability, the dark-state spectrum was normalized to the same SNR of the light one by applying a scaling factor of $\sqrt{\frac{NS_L}{NS_D}}$, and a linebroadening of 1 Hz for amino acids and 10~20 Hz for proteins was applied during the plotting. The detection limit for proteins is defined as the concentration at SNR ≥ 3 (10-Hz linebroadening).

1.5 Determination of Dissociation Constants by ^{19}F Photo-CIDNP NMR

Protein BD2 (5 μM) in Photo-CIDNP buffer containing 20 μM FL was titrated with GSK-778 at final concentrations of 0, 0.25, 1, 2.5, 4, 5.5, 8.5, 10, 11.5, 13 and 15 μM. After incubating each sample for at least 0.5 h at 25 °C, ^{19}F NMR spectra were acquired with 512 scans using a 0.2 s illumination period per scan. For each titration point, the ^{19}F intensity of free-state BD2 at the total GSK-778 concentration [L], denoted as I_C, was measured. The concentration of the protein-ligand complex, [PL], was calculated using the equation:

$$[\mathrm{PL}] = [\mathrm{P}]_{\mathrm{total}} \times (1 - I_C / I_0)$$

where I_0 is the ^{19}F intensity in the absence of GSK-778, and $[\mathrm{P}]_{\mathrm{total}}$ is the total protein concentration of BD2. The K_D was obtained by fitting the data to the following equation:

$$[PL] = \frac{[\mathrm{P}]_{total} + [\mathrm{L}] + K_D - \sqrt{([\mathrm{P}]_{total} + [\mathrm{L}] + K_D)^2 - 4[\mathrm{P}]_{total} \times [\mathrm{L}]}}{2}$$

1.6 DFT Calculations

All density functional theory (DFT) calculations were performed using Gaussian 16 software.[5] Geometry optimizations were conducted at the UB3LYP/6-311+G(2d,p) level. The g-factors and electron spin densities were calculated at the m062x/def2tzvp level.

2 Supplementary Figures and Tables

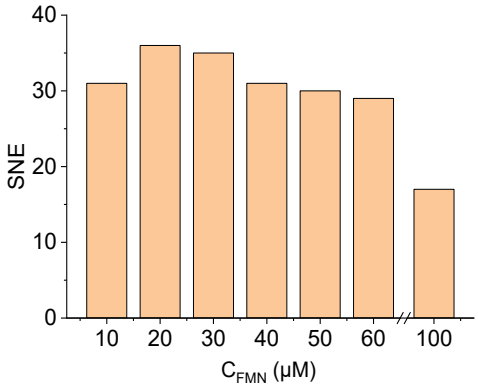

Figure S1 SNEs of ^{19}F for 6-F Trp (30 μM) as a function of FMN concentration. Under the experimental conditions (488 nm, 1.28 W, 1.5 s), the best performance was achieved at an FMN concentration of approximately 20 μM with 1 scan.

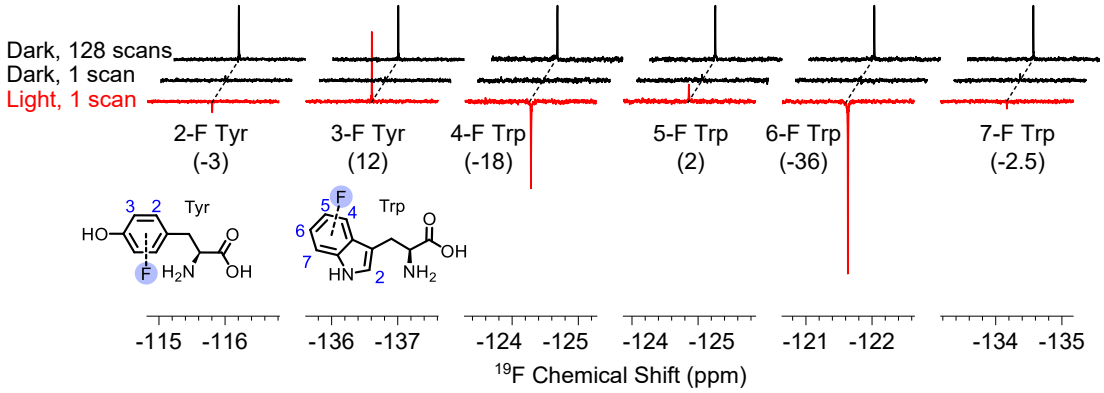

Figure S2 ^{19}F NMR spectra of monofluorinated Trp and Tyr (~30 μM) in the presence of FMN (20 μM).

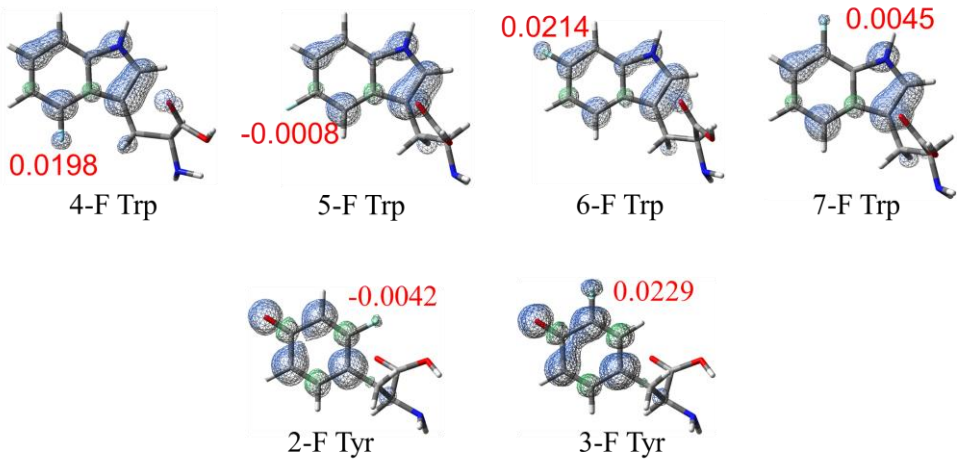

Figure S3 Electron spin density distributions of the monofluorinated Trp and Tyr radicals (isosurface value: 0.003). The Mulliken spin density on each ^{19}F is indicated with red numbers. Detailed spin density data are provided in Tables S1 and S2.

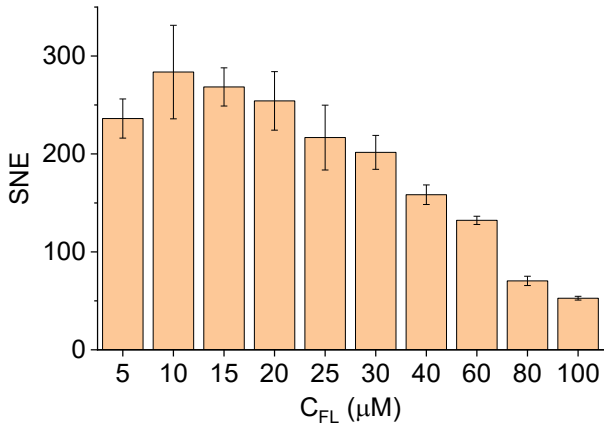

Figure S4 SNEs of ^{19}F for 6-F Trp (30 μM) as a function of FL concentration. Under the experimental conditions (488 nm, 1.28 W, 1.5 s), the best performance was achieved at an FL concentration of approximately 10 μM with 1 scan.

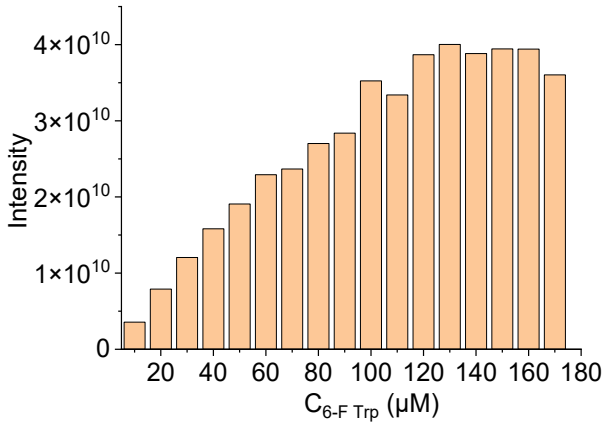

Figure S5 Concentration-dependent ^{19}F NMR intensity of 6-F Trp (30 μM) in the presence of FL (10 μM). The ^{19}F NMR signal intensity increases with 6-F Trp concentration and saturates at approximately 120 μM under the experimental conditions.

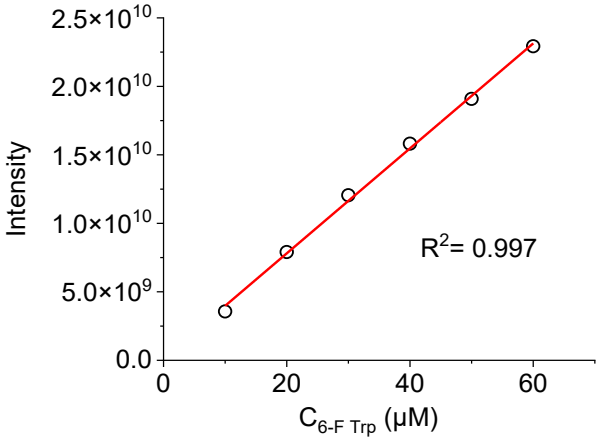

Figure S6 Plot of ^{19}F NMR signal intensity versus 6-F Trp concentration. The signal intensity increases linearly with concentration (R^2>0.99) in the range of 1–60 μM under the experimental conditions.

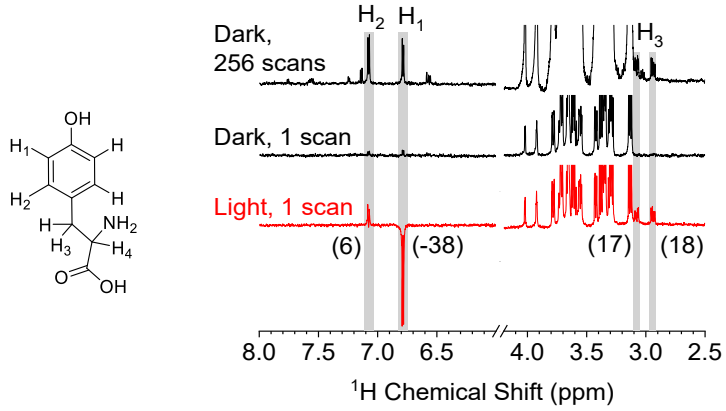

Figure S7 ^{1}H NMR spectra of the Tyr (30 μM) in photo-CIDNP buffer. The H_4 resonance (~3.95 ppm) was not assigned due to low intensity.

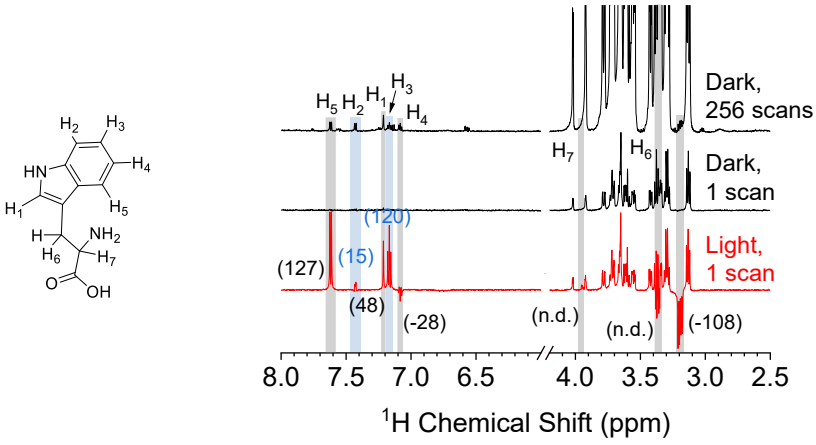

Figure S8 ^{1}H NMR spectra of the Trp (30 μM) in photo-CIDNP buffer. The SNE of H_7 at 3.96 ppm was not determined due to insufficient signal intensity.

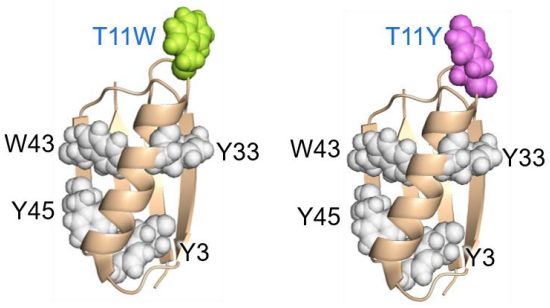

Figure S9 Structural illustration of the GB1 mutants T11W and T11Y (based on PDB: 2MQT), highlighting the locations of endogenous Trp and Tyr residues as well as the introduced mutations. The mutant structures were generated using Chimera.[6]

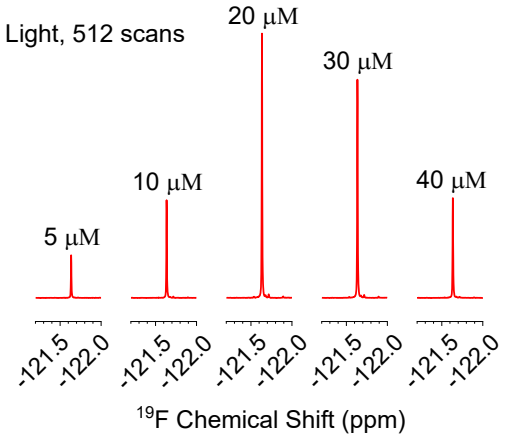

Figure S10 ^{19}F NMR spectra of 6-F Trp (30 μM) at varying FL concentrations. With 512 scans, an FL concentration of 20 μM yielded the best polarization performance.

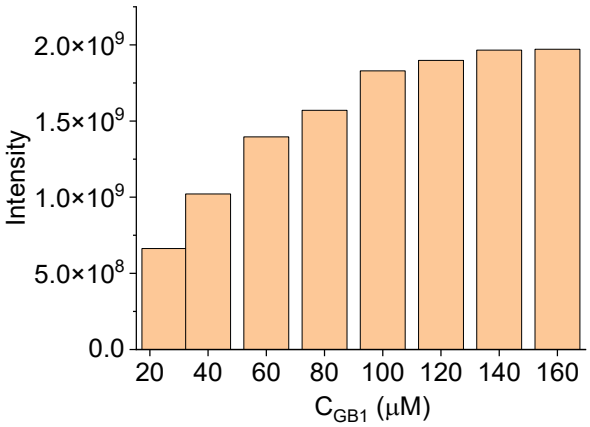

Figure S11 Concentration-dependent ^{19}F NMR intensity of GB1(T11W) incorporating 6-F Trp. The ^{19}F NMR signal intensity increases with protein concentration and saturates at approximately 140 μM under the experimental conditions.

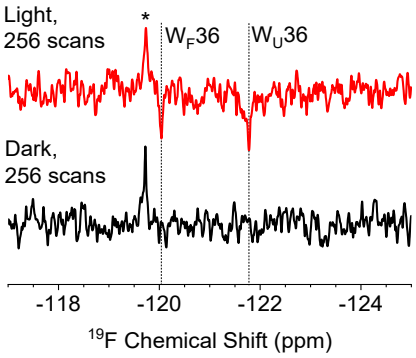

Figure S12 ^{19}F NMR spectra of 6-F Trp-labeled SH3 (1.0 μM). *Signal from F^- ion.

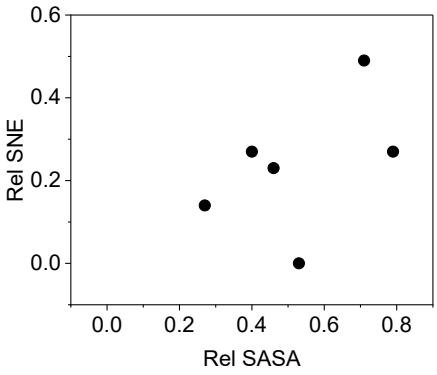

Figure S13 Plot of relative SNE (rel SNE) against relative solvent-accessible surface area (rel SASA) of side chains. Source data are provided in Table S3.

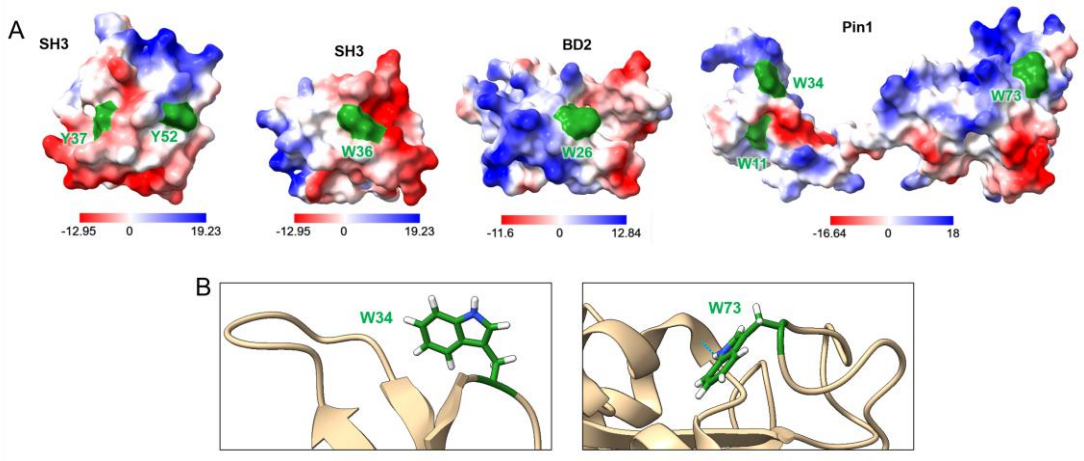

Figure S14 (A) Electrostatic surface potentials of SH3 (2A36, model 1), BD2 (7USK), and Pin1 (1NMV, model 1). (B) Comparison of the orientations of Trp34 and Trp73 in Pin1 (1NMV, model 1). Generated with Chimera.

As shown in Figures S13, S14, and Table S3, high solvent accessibility and a positively charged microenvironment (fluorescein is negatively charged) favor efficient polarization, as seen in SH3 and BD2. Nevertheless, W73 of Pin1 is an exception: despite its large SASA (0.53), it shows no photo-CIDNP activity, likely because its inward-oriented indole ring hinders electron transfer with fluorescein. This underscores that side-chain orientation and local interactions are also critical determinants of photo-CIDNP efficiency. Analysis of Trp–FL interactions in PDI was precluded by signal overlap.

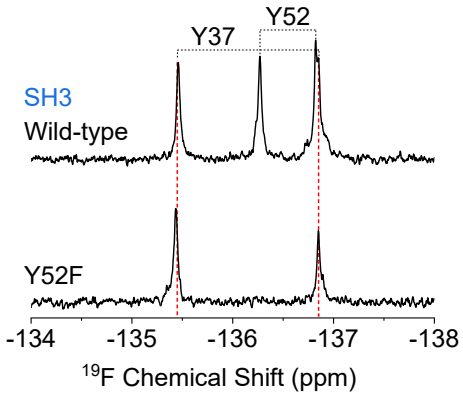

Figure S15 ^{19}F NMR spectra of 3-F Tyr-labeled wild-type and Tyr-to-Phe point mutated SH3.

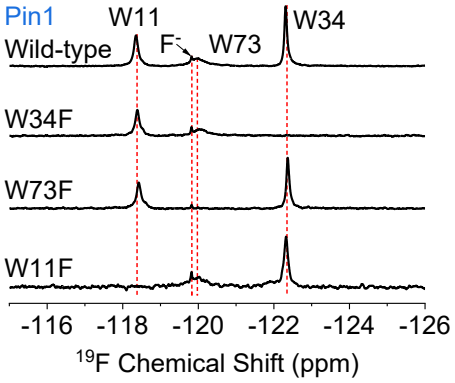

Figure S16 ^{19}F NMR spectra of 6-F Trp-labeled wild-type and Trp-to-Phe point mutated Pin1.

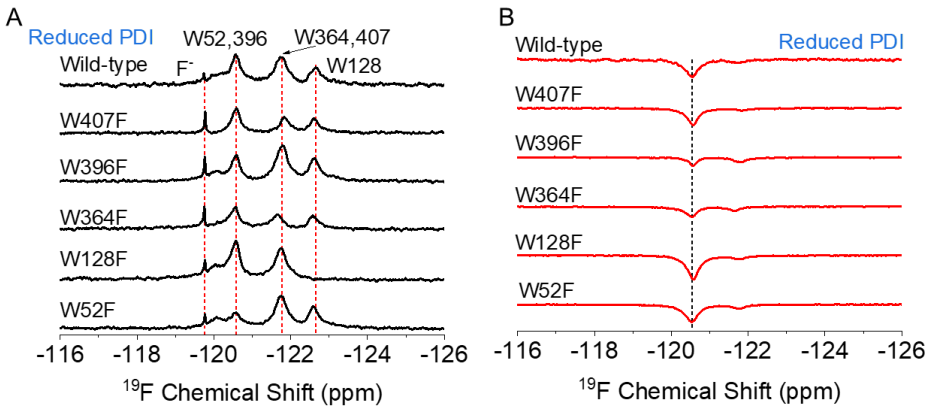

Figure S17 ^{19}F NMR spectra of 6-F Trp-labeled wild-type and Trp-to-Phe point mutated PDI (reduced state) in the dark (A) and upon illumination (B). Enhanced signals in both the W52F and W392F mutants indicate photo-CIDNP activity at the W52 and W392 sites.

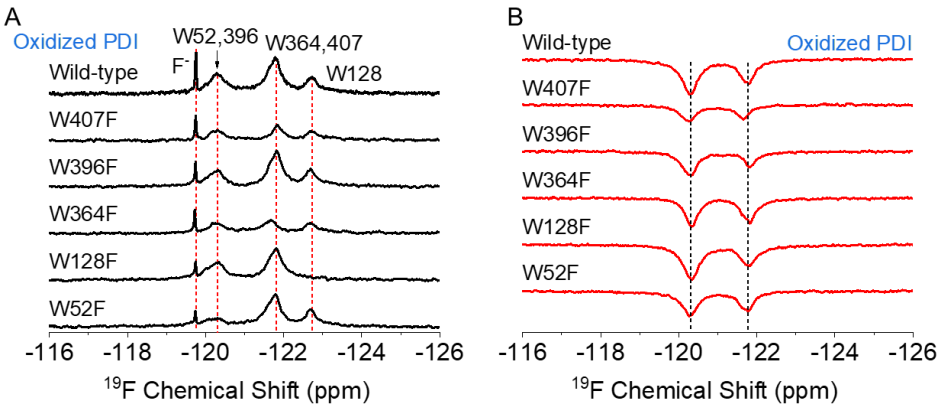

Figure S18 ^{19}F NMR spectra of 6-F Trp-labeled wild-type and Trp-to-Phe point mutated PDI (oxidized state) in the dark (A) and upon illumination (B). Enhanced signals in both the W52F and W392F mutants indicate photo-CIDNP activity at the W52 and W392 sites, with similar phenomena observed for W364 and W407.

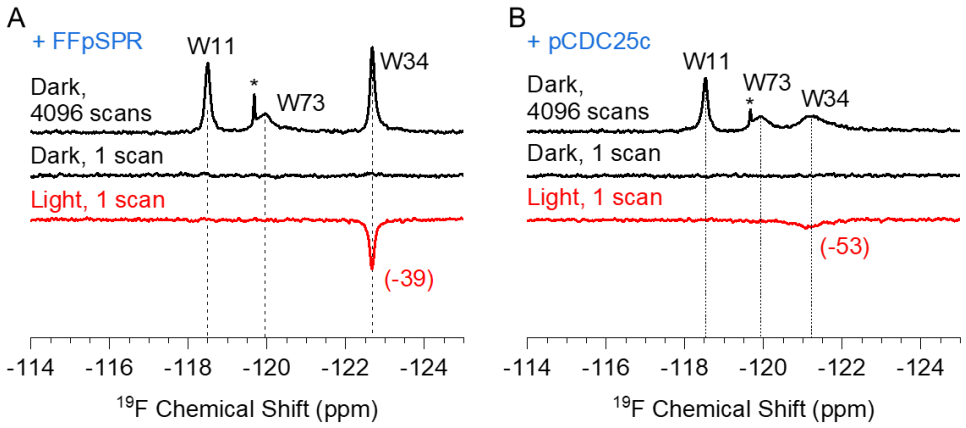

Figure S19 ^{19}F NMR spectra of 6-F Trp-labeled Pin1 with different substrates: (A) FFpSPR and (B) pCDC25c (each at 3 equivalents). *Signal from F^- ion.

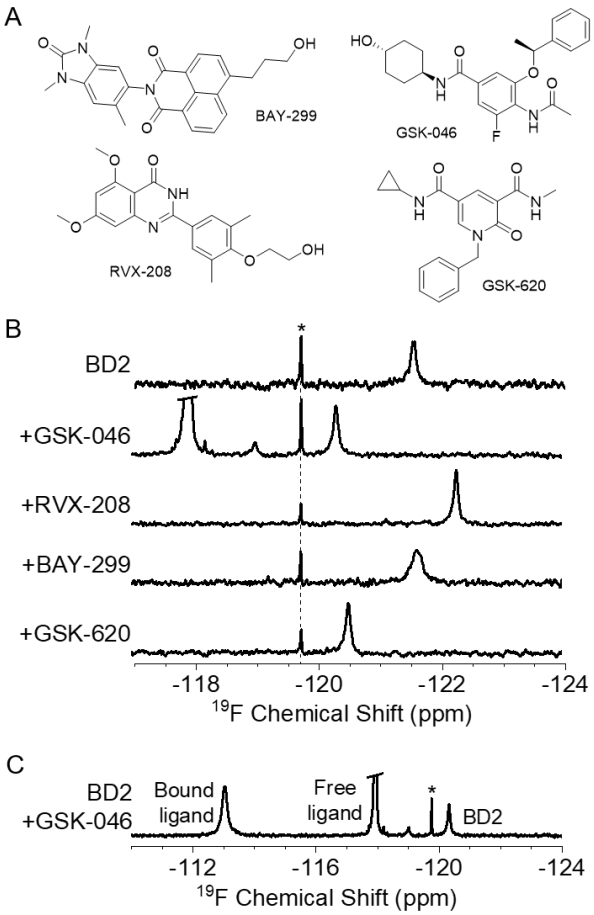

Figure S20 (A) Chemical structures of ligands. (B) ^{19}F NMR spectra of 6-F Trp-labeled BD2 in the presence of different ligands (3 equiv) in the dark. (C) Full ^{19}F NMR spectrum of 6-F Trp-labeled BD2 with GSK-046. *Signal from F^- ion.

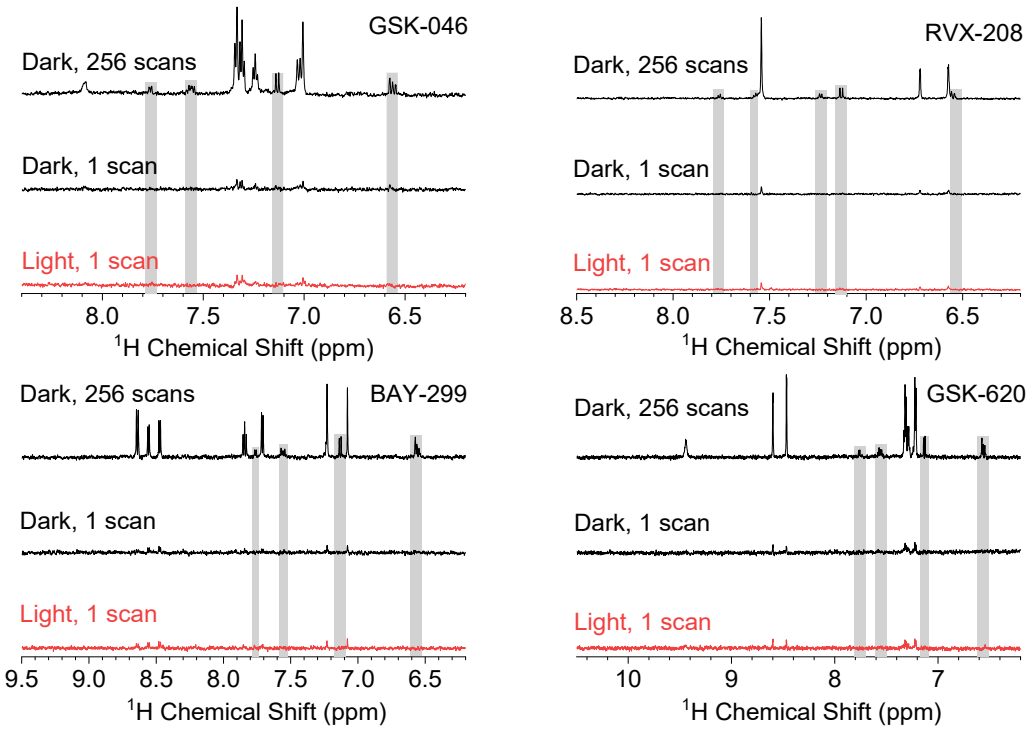

Figure S21 ^{1}H NMR spectra (aromatic region) of GSK-046, RVX-208, BAY-299 and GSK-620. Fluorescein signals (if resolved) are highlighted. None of these ligands are photo-CIDNP active.

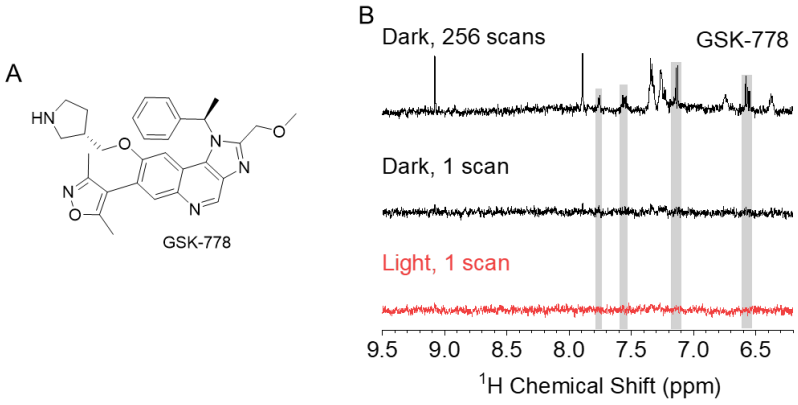

Figure S22 (A) Chemical structure of GSK-778. (B) ^{1}H NMR spectra (aromatic region) of GSK-778. Fluorescein signals (if resolved) are highlighted. No polarized signals were observed for any of the resonances.

Table S1 Atom labels and Mulliken spin densities (au) for tryptophan and monofluorotryptophan radicals.

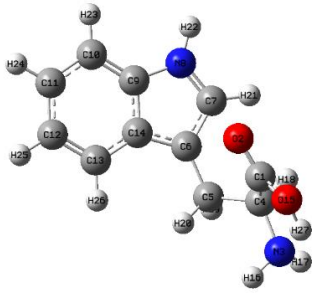

Trp

g_{iso}=2.0029

1C	-0.003601	15O	0.003447
2O	0.054649	16H	-0.000226
3N	0.007219	17H	-0.000474
4C	0.022001	18H	-0.00068
5C	-0.008046	19H	0.026289
6C	0.396468	20H	0.002598
7C	0.172645	21H	-0.006996
8N	0.125205	22H	-0.006311
9C	0.052967	23H	0.000335
10C	0.011906	24H	-0.003688
11C	0.162217	25H	0.000368
12C	-0.0837	26H	-0.004329
13C	0.179905	27H	-0.0006
14C	-0.099567		

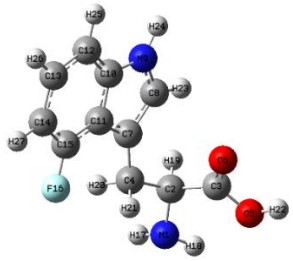

4-F Trp

g_{iso}=2.0032

1N	0.001836	15C	0.189659
2C	0.006476	16F	0.01984
3C	-0.000282	17H	-0.000196
4C	-0.013266	18H	-0.00019
5O	0.001877	19H	-0.002184
6O	0.018942	20H	0.027814
7C	0.373579	21H	0.015514
8C	0.164999	22H	0.000288
9N	0.130154	23H	-0.008592
10C	0.024664	24H	-0.006638
11C	-0.085155	25H	-0.000016
12C	0.056129	26H	-0.003844
13C	0.155925	27H	-0.000251
14C	-0.067082		

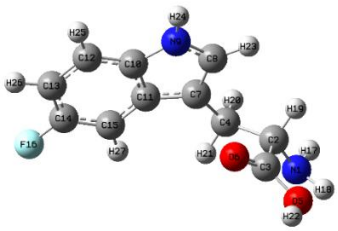

5-F Trp

g_{iso}=2.0029

1N	0.001702	15C	0.177302
2C	0.024101	16F	-0.000799
3C	-0.003185	17H	-0.000121
4C	-0.01576	18H	0.000308
5O	0.002785	19H	-0.002557
6O	0.031954	20H	0.031698
7C	0.440802	21H	0.004306
8C	0.147657	22H	0.000433
9N	0.160732	23H	-0.006788
10C	0.029304	24H	-0.007943

	11C	-0.091988	25H	0.000302
	12C	0.02592	26H	-0.003101
	13C	0.111856	27H	-0.004647
	14C	-0.054275		

	1N	0.001642	15C	0.161916
	2C	0.013208	16F	0.021377
	3C	-0.00108	17H	-0.000152
	4C	-0.013692	18H	-0.000001
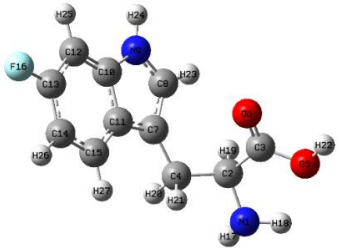	5O	0.002275	19H	-0.001996
	6O	0.024927	20H	0.026411
	7C	0.33147	21H	0.007791
	8C	0.231277	22H	0.000304
	9N	0.0959	23H	-0.00904
6-F Trp	10C	0.079579	24H	-0.005283
g_{iso}=2.0032	11C	-0.07939	25H	-0.000437
	12C	0.018892	26H	0.000515
	13C	0.191733	27H	-0.003994
	14C	-0.094153		

	1N	0.001489	15C	0.221237
	2C	0.025203	16F	0.004496
	3C	-0.00409	17H	-0.000097
	4C	-0.015864	18H	0.000318
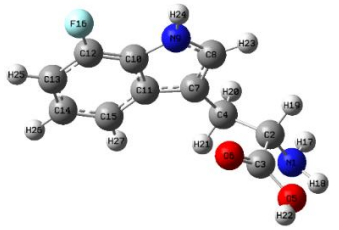	5O	0.002388	19H	-0.002856
	6O	0.028251	20H	0.028458
	7C	0.401443	21H	0.003486
	8C	0.138336	22H	0.000371
	9N	0.16113	23H	-0.006318
7-F Trp	10C	0.013704	24H	-0.007984
g_{iso}=2.0030	11C	-0.09898	25H	-0.003325
	12C	0.034089	26H	-0.000099
	13C	0.156535	27H	-0.004602
	14C	-0.076721		

Table S2 Atom labels and Mulliken spin densities (au) for tyrosine and monofluorotyrosine radicals.

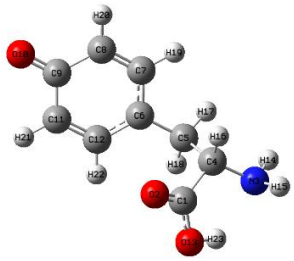 Tyr g_{iso}=2.0097	1C	0.000179	13O	0.000349
	2O	0.001028	14H	0.000556
	3N	0.001914	15H	0.0003
	4C	0.022053	16H	-0.004446
	5C	-0.030017	17H	0.008325
	6C	0.471761	18H	0.00251
	7C	-0.192287	19H	0.001713
	8C	0.329952	20H	-0.00757
	9C	-0.134333	21H	-0.007542
	10O	0.397109	22H	0.00241
	11C	0.336423	23H	-0.000035
	12C	-0.200351		

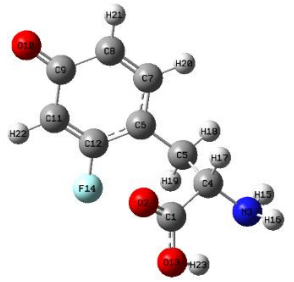 2-F Tyr g_{iso}=2.0091	1C	-0.001242	13O	0.000618
	2O	0.002558	14F	-0.004195
	3N	0.001715	15H	0.000608
	4C	0.02399	16H	0.000318
	5C	-0.031359	17H	-0.003776
	6C	0.471048	18H	0.007857
	7C	-0.195745	19H	0.003361
	8C	0.364145	20H	0.002192
	9C	-0.134007	21H	-0.008474
	10O	0.386293	22H	-0.006126
	11C	0.278026	23H	-0.00004
	12C	-0.157763		

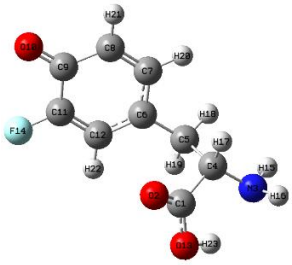 3-F Tyr g_{iso}=2.0084	1C	-0.001035	13O	0.000389
	2O	0.001407	14F	0.022899
	3N	0.001883	15H	0.000571
	4C	0.022874	16H	0.000292
	5C	-0.027212	17H	-0.00488
	6C	0.434474	18H	0.008791
	7C	-0.163155	19H	0.001852
	8C	0.2744	20H	0.000756
	9C	-0.094645	21H	-0.006262
	10O	0.388289	22H	0.00287
	11C	0.321917	23H	-0.000037
	12C	-0.186437		

Table S3 Relative solvent-accessible surface area and SNEs of different proteins.

Protein (PDB ID)	Residue	Rel SASA[a]	Rel SNE[g]
SH3 (2A36) [b]	W36	0.46	0.23
	Y37	0.27	0.14
	Y52	0.40	0.27
Pin1 (1NMV) [b]	W11	0.16	n.d.[e]
	W34	0.79	0.27
	W73	0.53	n.d.
Reduced PDI[c] (4EKZ)	W52/W396	0.85/0.41	0.27[f]
	W128	0.12	n.d
	W364/W407	0.34/0.01	0.10[f]
Oxidized PDI[c, d] (4EL1)	W52/W396	0.85/0.55	0.28[f]
	W128	0.07	n.d.
	W364/W407	0.39/0.18	0.09[f]
BD2 (7USK) [c]	W26	0.71	0.49

[a] Relative solvent-accessible surface area (rel SASA) of side chains calculated using a 0.14 nm probe (water) (FreeSASA[7]). [b] Solution structure from NMR; average SASA over all models. [c] Crystal structure from X-ray. [d] Single chain extracted from the unit cell. [e] Not determined due to photo-CIDNP silence under the experimental conditions. [f] Not assigned to individual residues due to signal overlap. [g] Rel SNE = $SNE_{protein}$ / $SNE_{free\ probe}$.

3 Supplementary References

1 Crowley, P. B.; Kyne, C.; Monteith, W. B. Simple and Inexpensive Incorporation of ^{19}F-Tryptophan for Protein NMR Spectroscopy. *Chem. Commun.* **2012**, *48* (86), 10681-10683.

2 Li, C.; Wang, G.-F.; Wang, Y.; Creager-Allen, R.; Lutz, E. A.; Scronce, H.; Slade, K. M.; Ruf, R. A. S.; Mehl, R. A.; Pielak, G. J. Protein ^{19}F NMR in Escherichia Coli. *J. Am. Chem. Soc.* **2010**, *132* (1), 321-327.

3 Okuno, Y.; Mecha, M. F.; Yang, H.; Zhu, L.; Fry, C. G.; Cavagnero, S. Laser- and Cryogenic Probe-Assisted NMR Enables Hypersensitive Analysis of Biomolecules at Submicromolar Concentration. *Proc. Natl. Acad. Sci. U.S.A.* **2019**, *116* (24), 11602-11611.

4 Chai, Z.; Wang, W.; Chen, J.; Wu, Q.; Ma, L.; Liu, Z.; Xu, G.; Jiang, L.; Shu, Y.; Liu, M.; Li, C. Expanding the Molecular Scope of Photo-CIDNP for Nanomolar ^{19}F NMR Detection of Amines. *J. Am. Chem. Soc.* **2026**, *148* (9), 9213-9218.

5 Gaussian 16, R. C. M. J. F., G. W. Trucks, H. B. Schlegel, G. E. Scuseria, ; M. A. Robb, J. R. C., G. Scalmani, V. Barone, ; G. A. Petersson, H. N., X. Li, M. Caricato, A. V. Marenich, ; J. Bloino, B. G. J., R. Gomperts, B. Mennucci, H. P. Hratchian, ; J. V. Ortiz, A. F. I., J. L. Sonnenberg, D. Williams-Young, ; F. Ding, F. L., F. Egidi, J. Goings, B. Peng, A. Petrone, ; T. Henderson, D. R., V. G. Zakrzewski, J. Gao, N. Rega, ; G. Zheng, W. L., M. Hada, M. Ehara, K. Toyota, R. Fukuda, ; J. Hasegawa, M. I., T. Nakajima, Y. Honda, O. Kitao, H. Nakai, ; T. Vreven, K. T., J. A. Montgomery, Jr., J. E. Peralta, ; F. Ogliaro, M. J. B., J. J. Heyd, E. N. Brothers, K. N. Kudin, ; V. N. Staroverov, T. A. K., R. Kobayashi, J. Normand, ; K. Raghavachari, A. P. R., J. C. Burant, S. S. Iyengar, ; J. Tomasi, M. C., J. M. Millam, M. Klene, C. Adamo, R. Cammi, ; J. W. Ochterski, R. L. M., K. Morokuma, O. Farkas, ; J. B. Foresman, a. D. J. F., Gaussian, Inc., Wallingford CT, 2019.

6 Pettersen, E. F.; Goddard, T. D.; Huang, C. C.; Couch, G. S.; Greenblatt, D. M.; Meng, E. C.; Ferrin, T. E. UCSF Chimera—A Visualization System for Exploratory Research and Analysis. *J. Comput. Chem.* **2004**, *25* (13), 1605-1612.

7 Mitternacht, S. FreeSASA: An Open Source C Library for Solvent Accessible Surface Area Calculations. *F1000Res* **2016**, *5*, 189.